A Macroscale-Mesoscale Numerical Model of Intense Baroclinic Development[1]

MICHAEL L. KAPLAN[2]
Dept. of Atmospheric Science, State University of New York at Albany
AND DOUGLAS A. PAINE
Division of Atmospheric Sciences, Cornell University, Ithaca, N. Y.

(Manuscript received 8 May 1972, in revised form 25 July 1972)

ABSTRACT

A numerical model has been designed to link quasi-geostrophic and mesoscale forcing. Initializations performed at 127 km with either a barotropic forecast or a diagnostic omega equation are followed by a prediction with a moist nine-level primitive equation model operating on a 32-km grid mesh. The results of two short-period integrations indicate good correspondence between forecast omega fields and radar observations, observed snowfall, and diagnostic integrations. Vertical motions reach maxima of 25 and 50 cm sec^{-1}, while the forecast dependent variables indicate an integral role played by long gravity waves in organizing mesoscale development.

1. Introduction

Petterssen's (1956) classic work on atmospheric development created a school of meteorological thought which stressed the importance of the superposition of hydrodynamic and thermodynamic forcing functions leading to the local production of vorticity. Petterssen, however, tacitly assumed that the energy stored at smaller scales, while contributing to development, was not the prime energy source. In an effort to numerically simulate intense mesoscale phenomena, we must include energy at several scales of motion, as well as a means for the transfer of this energy through the wave spectrum. A numerical model discussed in this paper simulates this nonlinear interaction, while permitting the evaluation of the importance of each forcing function during severe atmospheric development.

2. Physical model

The physical model consists of two parts: first, an initial atmospheric state, and second, a prognostic state. The initial atmospheric state is determined by either a ten-level quasi-geostrophic diagnostic omega equation or a single-level equivalent barotropic forecast. The ten-level diagnostic model utilizes a 127-km horizontal grid mesh (shown in Fig. 1) and subjectively analyzed geopotential height (Z) fields, temperatures (T), and relative humidities at 950 through 150 mb to determine values of vertical velocity at levels 900 to 200 mb. The initial fields may also be approximated by first solving a barotropic forecast equation at the 850-mb level. Values of the dependent variables including the mixing ratio (Q), T and Z are then calculated from this forecast height field by assuming a vertical profile of temperature and relative humidity from representative radiosonde data. These initial fields are used as a first approximation for the dependent variables used in a primitive equation model.

The prognostic model has levels (listed in the table)

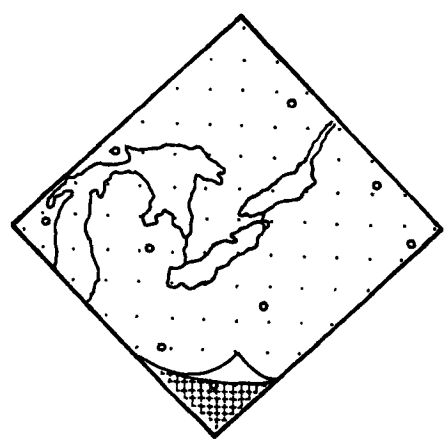

FIG. 1. A portion of the 127-km grid mesh (dots) used for determining quasi-geostrophic forcing, plus the 32-km mesoscale grid (crosses) and area of integration of the P.E. model. Circles represent radiosonde locations.

[1] Presented at the Fourth Conference on Weather Forecasting and Analysis, 1–4 May 1972, Portland, Ore.
[2] Present affiliation: Air Force Global Weather Central, Offutt Air Force Base, Omaha, Nebr.

Unauthenticated | Downloaded 06/15/24 06:48 AM UTC

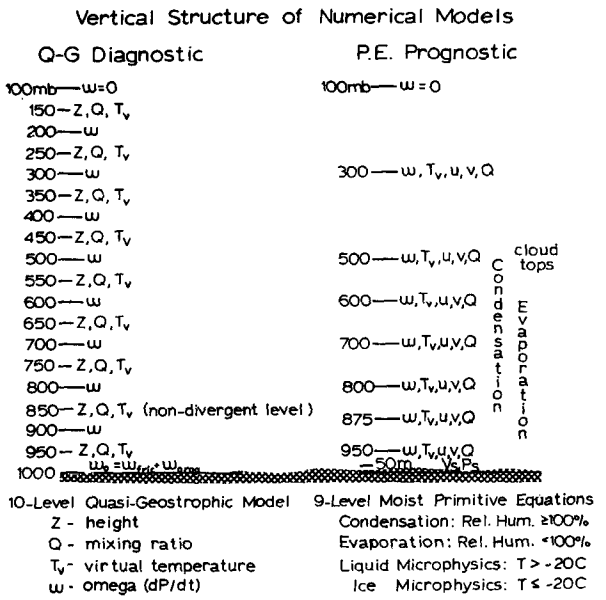

at 50 m above the surface, and at 950, 875, 800, 700, 600, 500, 300 and 100 mb. The emphasis on lower tropospheric vertical resolution is due to a desire to simulate the important low-level contribution of heat, moisture and momentum as well as latent heat release. The horizontal grid distance is approximately 32 km and the area of integration seen in Fig. 1 covers most of the eastern Great Lakes, New York, Pennsylvania, Ohio, and southeastern Canada.

3. Equations

In an effort to determine the initial vertical motion field from the information contained in the geopotential height data, one must perform a three-dimensional relaxation of the familiar quasi-geostrophic omega equation in the form

$$\left(\nabla^2+\frac{f^2}{\sigma}\frac{\partial^2}{\partial P^2}\right)\omega=-\frac{f}{\sigma}\frac{\partial}{\partial P}[-\mathbf{V}\cdot\nabla(\zeta+f)]+\frac{1}{\sigma}\nabla^2\left(-\mathbf{V}\cdot\nabla\frac{\partial\Phi}{\partial P}\right), \quad (1)$$

where the three-dimensional Laplacian of omega is determined by a forcing function consisting of the vertical variation of the vorticity advection and the Laplacian of the geopotential thickness advection. This relaxation procedure requires vertical and lateral boundary conditions for omega. The lateral boundary values of omega are set equal to zero at every level (Stuart and O'Neill, 1967). The 100-mb boundary value of omega is also set equal to zero, while the 1000-mb omega is assumed equal to the summation of a frictional and orographic contribution. The orographic contribution may be calculated in the following manner:

$$\omega_{\text{orog}}=\mathbf{V}\cdot\nabla P_s, \quad (2)$$

in which P_s represents subjectively analyzed values of surface pressure. Additional symbols are defined in Appendix A. The frictional contribution

$$\omega_{\text{fric}}=\frac{\rho g}{fd}(\tau_x-\tau_y), \quad (3)$$

is based on subjectively analyzed values of surface wind velocity and direction (Thompson, 1961). These two functions yield a total surface boundary contribution to omega of

$$\omega_{1000}=\omega_{\text{orog}}+\omega_{\text{fric}}. \quad (4)$$

Since this problem concerns the alteration of an initial quasi-geostrophic fluid by smaller scale baroclinic energy sources, the initial vertical motions should include the effects of this energy input which have taken place up to time zero. A method for including the alteration of initial omega fields due to static stability variations is utilized. Following Sanders and Olson (1967), we allow modification of the omega fields without violation of the ellipticity conditions of the partial differential equation in the conditionally unstable atmosphere. Mathematically, this enhancement factor may be expressed

$$\frac{\omega_R}{\omega_I}=-\frac{1+\sigma_I\dfrac{(1/A^2+1/B^2)}{f^2}C^2}{1+\sigma_R\dfrac{(1/A^2+1/B^2)}{f^2}C^2}, \quad (5)$$

where the subscripts I and R refer to the ideal or standard atmosphere and the real atmosphere, respectively. The static stability σ_I of the standard atmosphere is derived from appropriate climatological values of σ, while σ_R is calculated from real values of temperature and relative humidity by means of the relationship

$$\sigma_R=-\frac{RT}{\theta_e P}\frac{\partial\theta_e}{\partial P}, \quad (6)$$

in which θ_e is approximated by the static energy (after Kreitzberg and Brown, 1970):

$$\theta_e\approx T+\frac{LQ}{C_p}+\frac{gZ}{C_p}. \quad (7)$$

The use of this enhancement factor allows one to alter the initial omegas as a function of the static stability variations resulting from low-level heat and moisture flux. Because the enhancement factor is based upon the quasi-geostrophic assumption, it is applied only in the lower third of the atmosphere away from the ageostrophy of the jet core.

Unauthenticated | Downloaded 06/15/24 06:48 AM UTC

The second method of providing an initial omega field consists of solving a single-level barotropic forecast model at the 127-km grid scale and then making the appropriate assumptions concerning the vertical variation of the slope of the constant pressure surfaces. The forecast equation

$$\nabla^2\frac{\partial Z}{\partial t}=-\tfrac{1}{4}[J(Z,\zeta+f_0)_{\mathrm{lnd}}], \tag{8}$$

is solved at an assumed level of non-divergence (lnd). Paine and Kaplan (1971) and Paine (1971) have shown that when low-level energy flux is a significant contributor to development, often a second level of non-divergence exists in the lower troposphere. One may solve for an initial vertical stratification of vertical motion in the lower troposphere by assuming the boundary conditions

$$\omega_{1000}=0, \quad \omega_{700}=\tfrac{1}{2}\omega_{850}, \tag{9}$$

and then integrating the equation of continuity in the form

$$\left.\frac{2\mathbf{V}\cdot\nabla(\zeta_{\mathrm{lnd}}+f_0)}{\zeta_{\mathrm{lnd}}+f_0}\right|_{1000}^{700}\partial P=\int_{\mathrm{lnd}}^{700}\partial\omega+\int_{1000}^{\mathrm{lnd}}\partial\omega, \tag{10}$$

where the level of non-divergence is 850 mb. A parabolic profile of omega is assumed to exist in the mid and upper troposphere. Although this initialization procedure is only an approximation, it can provide the nine-level prognostic model with a real-time forecast of upward increasing positive vorticity advection which aids in liberating the energy stored at smaller atmospheric scales.

The nine-level prognostic model employs a full set of the primitive equations. The dependent variables are total water substance (liquid and gaseous) Q; temperature T; horizontal wind components u,v; and surface pressure P_s. The diagnostic equations employed determine the virtual temperature T_v; geopotential height Z; and the vertical velocity ω.

The equations are discussed in their order of integration. The moisture conservation equation is

$$\frac{\partial Q}{\partial t}=-m(\mathbf{V}\cdot\nabla Q)-\omega\frac{\partial Q}{\partial P}-C_1+C_2, \tag{11}$$

in which C_1 is the low-level moisture flux term solved only at 950 mb; and is expressed in the form

$$C_1=\left\{\frac{K_Q}{K_M}\frac{C_d}{2}[(u^2_{950}+v^2_{950})^{\frac{1}{2}}+(u^2_{sfc}+v^2_{sfc})^{\frac{1}{2}}]\right\}\times\frac{Q-Q_{sfc}}{Z-Z_{sfc}}, \tag{12}$$

where all heat and moisture flux processes are assumed for a well-mixed fluid between 950 mb and the surface. This form of the bulk aerodynamic flux is taken from Lavoie (1968) with the following two modifications: first, a mean stress is used to incorporate the momentum fields of both the 950 mb and 50 m surfaces, and second, the ratios of the eddy transport terms (K_Q/K_M) are assumed equal to unity in lieu of the scale of the model.

Term C_2 is the condensation or evaporation term. Condensation is permitted at levels from 875 through 500 mb, while evaporation may occur at levels from 950 through 600 mb. Since we are modeling the baroclinic input from warm water bodies in the cold season, the limited depth of convection allows restriction of cloud tops to 500 mb. Condensation is permitted at relative humidities $\geqslant 100\%$ with evaporation allowed at relative humidities $<100\%$. At temperatures $\leqslant -20$C, ice microphysical processes are assumed. The water storage is a function of temperature and supersaturation:

$$\text{storage}=Q-\{[(268.16-T)0.02]+0.1+[(Q-Q_{\mathrm{sat}})^{10}]\}. \tag{13}$$

This expression assumes a linear decrease of liquid storage per time step as a function of temperature, as well as the additive effect of a constant 10% release of condensate due to collision-coalescence effects. Both of these assumptions are arbitrary first approximations allowing between 80 and 40% storage of condensate as the temperature decreases from -5 to -20C, respectively. Preliminary integrations have allowed water condensate to fall one level per time step. This approximates a fall velocity of 7 m sec^{-1}, nearly three times the fall rate of heavy graupel or rimed crystals (Nakaya, 1954), allowing for a significant displacement of the predicted precipitation relative to the observed snowfall.

The temperature prognostic equation (thermodynamic energy equation) is

$$\frac{\partial T}{\partial t}=-m(\mathbf{V}\cdot\nabla T)-\omega\left(\frac{\partial T}{\partial P}-\frac{\alpha}{C_p}\right)-H_1+H_2, \tag{14}$$

where, at 950 mb, H_1 is analogous to term C_1 above, i.e.,

$$H_1=\left\{\frac{K_H}{K_M}\frac{C_d}{2}[(u^2_{950}+v^2_{950})^{\frac{1}{2}}+(u^2_{sfc}+v^2_{sfc})^{\frac{1}{2}}]\right\}\times\frac{T-T_{sfc}}{Z-Z_{sfc}}. \tag{15}$$

At 950 mb, $\omega(\partial T/\partial P-\alpha/C_p)$ is assumed equal to zero and above 950 mb,

$$\omega\left(\frac{\partial T}{\partial P}-\frac{\alpha}{C_p}\right)=\frac{L}{C_{pm}}\omega\frac{\partial Q_{\mathrm{sat}}}{\partial P}-\frac{RT}{PC_p}\omega. \tag{16}$$

Term H_2 is the latent heating or evaporative cooling expressed in the form

$$H_2=\frac{L}{C_{pm}}\Delta c, \tag{17}$$

Unauthenticated | Downloaded 06/15/24 06:48 AM UTC

where L is computed from

$$L=L_{\text{constant}}+[(C_{pm}-C_p)(T-273.16)], \quad (18)$$

and ΔC is the condensation rate. The virtual temperature is determined from

$$T_v=T(1+Q/0.622)(1+Q)^{-1}, \quad (19)$$

where Q is limited to gaseous moisture.

One may calculate the new height field by combining the hydrostatic relationship and ideal gas law, yielding

$$Z_{\text{level}}=Z_{\text{level}-1}-\frac{R\bar{T}_v}{g}\log\left(\frac{P_1}{P_2}\right), \quad (20)$$

where $\bar{T}_v$ is a mean virtual temperature.

The horizontal accelerations are then computed from the equations of motion:

$$\frac{\partial u}{\partial t}=-m(\mathbf{V}\cdot\nabla u)-\omega\frac{\partial u}{\partial P}+fv-m\frac{\partial \Phi}{\partial x}+F_x, \quad (21)$$

$$\frac{\partial v}{\partial t}=-m(\mathbf{V}\cdot\nabla v)-\omega\frac{\partial v}{\partial P}-fu-m\frac{\partial \Phi}{\partial y}+F_y, \quad (22)$$

where F_x and F_y are the frictional stresses computed by

$$\int_{sfc}^{950 \text{ or } 875 \text{ mb}} C_d u(u^2+v^2)^{\frac{1}{2}}\partial Z^{-1}, \quad (23)$$

$$\int_{sfc}^{950 \text{ or } 875 \text{ mb}} C_d v(u^2+v^2)^{\frac{1}{2}}\partial Z^{-1}, \quad (24)$$

after Lavoie (1968). The lifting condensation level and top of the Ekman layer are both assumed to be 875 mb.

The equation of continuity is next integrated via the trapezoidal rule to determine the vertical distribution of omega:

$$\frac{\partial \omega}{\partial p}=-m^2\nabla\cdot\mathbf{V}, \quad \sum_m^n f(x)dx=\frac{h}{2}f(x)_m + hf(x)_{m+1}+\cdots\frac{h}{2}f(x)_n, \quad (25)$$

where $f(x)$ represents the divergence, h a vertical pressure increment, and m and n the lower and upper bounds for the isobaric levels (Gerald, 1970).

The final differencing equation is the pressure tendency equation expressed in the form

$$\frac{\partial P_s}{\partial t}=-m(\mathbf{V}_s\cdot\nabla P_s)+w\frac{\partial P}{\partial Z}+\int_{P_{950}}^{P_{300}}\nabla\cdot\mathbf{V}dP, \quad (26)$$

where $\mathbf{V}_s$ is the boundary level wind (Bushby and Timpson, 1967).

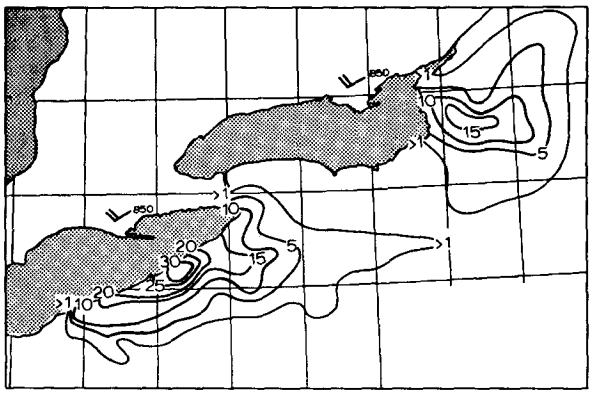

FIG. 2. Total snowfall during 4–7 November 1967. Isopleths are in inches.

4. Numerical method

Since the prime purpose of the numerical experiment is to simulate the nonlinear interaction among scales of motion in the atmosphere, the damping characteristics of the numerical scheme are critical to the success of the problem. The Euler-backward scheme (Matsuno, 1966) is employed because of its highly selective damping characteristics. Gerrity and McPherson (1970) have shown that this scheme damps the 2Δ waves most effectively at numerical stability ratios of approximately 1. If one assumes

$$g\approx 10 \text{ m sec}^{-2}, \quad \Delta X\approx 32 \text{ km}, \quad (27)$$

and a scale height H of the disturbance of ~ 3 km, then solution for the time step from the relationship for the stability ratio $[(gH)^{\frac{1}{2}}\Delta t/\Delta X]$ yields a $\Delta t\approx 185$ sec for neutral stability. This maximum damping of the 2Δ wave should be compared with the minimal damping of the initial synoptic-scale feature. This allows the initial large-scale motion to be altered in time by smaller scale energy sources. The damping of the 2Δ wave is not restricted to the temporal mode; the spatial mode is damped by applying a filter $\overline{u^{*xxyy}}$, where $u^*=\frac{1}{2}u^n$ for both components of the velocity field (McPherson, 1971). Thus, the quasi-geostrophic and mixed Rossby-gravity wave systems, ($\lambda\geqslant 128$ km) are allowed in the numerical solutions while restricting the 2Δ higher frequency gravitational modes.

The Euler-backward differencing scheme consists of a guess and then a correction to this guess, i.e.,

$$\epsilon^{*\tau+1}-\epsilon^{\tau}=f(\epsilon^{\tau})\Delta t, \quad (28)$$

$$\epsilon^{\tau+1}-\epsilon^{\tau}=f(\epsilon^{*\tau+1})\Delta t, \quad (29)$$

where ϵ is any dependent variable and starred variables represent first-guess values. This process tends to reduce the higher order solutions relative to the first- and second-order parts of the series.

The 36×32 grid point matrix used for the 32 km primitive equation forecast model is embedded within

Unauthenticated | Downloaded 06/15/24 06:48 AM UTC

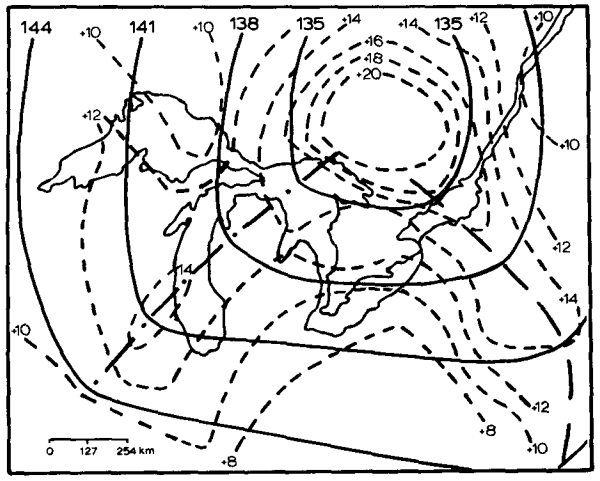

a.

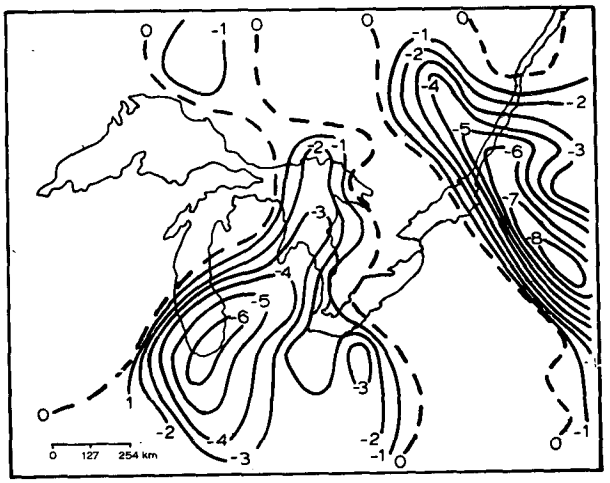

b.

FIG. 3. 850-mb forecast height (dm) and absolute vorticity ($\times 10^{-5}$ sec^{-1}), a., and 850-mb forecast ascent (μb sec^{-1}), b., both for 1800 GMT 4 November 1967.

the initialization grid by several hundred kilometers on all sides. The upstream boundary conditions (northwestern and southwestern walls) for the prognostic equations in Q, T, u, v are similar to those used for the barotropic forecast, i.e., each outside point is set equal to the first interior point at every time step. The outflow boundaries are handled after a method described by Nitta (1962) in which the boundary values of Q, T, u, v are set equal to twice the first interior grid point value minus the second interior grid point value at every time step. The pressure tendency equation is integrated with the first two interior rows maintained constant in time. The entire grid is rotated such that the maximum u velocity component is parallel to the southeastern boundary.

5. Synoptic situation

The synoptic situation to be utilized as the case study led to a series of intense lake-induced snowfalls affecting the areas east of Lake Erie and Lake Ontario. Locally, snowfall greater than 30 inches was recorded during the period from 4–7 November 1967 (Fig. 2), with most of the precipitation falling early in the storm period. Paine and Kaplan (1971) have shown evidence that this snowfall is the result of interaction which took place between a synoptic-scale trough and the elongated mesoscale heat sources shaped by the geometry of the warm water bodies. Simpson (1968) has reported on a similar case of severe atmospheric development produced by the interaction between a cold synoptic-scale wave and the warm waters of the North Pacific.

At 1800 GMT 4 November, a low pressure center was moving eastward from south of Hudson Bay, with its cold front entering western New England. Behind this front, a weak trough with a wavelength of ~1000 km was forecast by an equivalent barotropic model (Paine and Kaplan, 1971) to lie just west of Lake Erie as it crossed Lake Huron. This secondary feature shown as a dot-dash line in Fig. 3a had a maximum amplitude between 800 and 900 mb, and was preceded by a cold surge of arctic air some 25F colder at the surface than the waters of Lakes Erie and Ontario.

6. Results of numerical integrations

a. Initial data

The 1200 GMT 4 November 850-mb height field was used as initial data for the 6-hr barotropic forecast. In addition, the ten-level quasi-geostrophic omega equation was integrated for 0000 on 5 November. These provide two sources of initial data from the 127-km grid scale which are reduced to the 32-km grid to be used as initial data for the nine-level P. E. model.

The dependent variables are linearly interpolated down to the 32-km scale and to the appropriate levels in the P. E. model. The temperature of both lakes is assumed to be 10K warmer than the surrounding land areas, and the surface values of Q are assumed to be 90% of the saturation mixing ratio at the lake surface. Between the surface and 50 m levels is a zone of intense

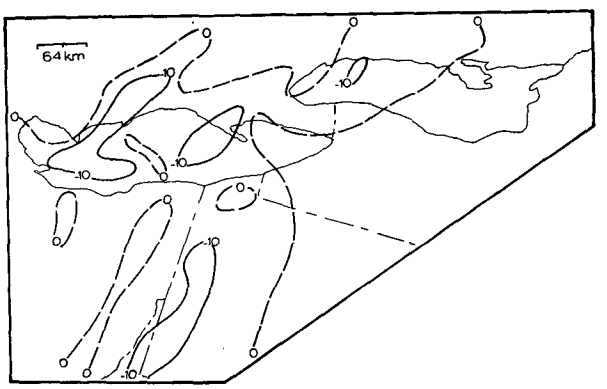

FIG. 4. 950-mb omegas (μb sec^{-1}) forecast at 6 hr beyond the initialization by the 127-km barotropic model.

Unauthenticated | Downloaded 06/15/24 06:48 AM UTC

vertical gradients of heat, moisture and momentum surmounted by a well-mixed layer between 50 m and 950 mb (Lavoie, 1968). The drag coefficient varies consistently from 0.0016 over the lake surface to 0.40 over the land areas. The values of surface topography are restricted to lie beneath 950 mb and are smoothed using a nine-point filter (Shuman, 1957). The terrain contribution to the omega field is $-(\mathbf{V}\cdot\nabla Z_0)\rho g$, where $\mathbf{V}$ is the 950-mb wind. This terrain-induced omega serves as part of the lower boundary condition for the model.

The barotropically forecast absolute vorticity field shown in Fig. 3a indicates that at 1800 GMT 4 November, the western half of Lakes Erie and Ontario are just coming under the influence of positive vorticity advection. This induces an environment favorable for intense vertical transport of heat and moisture as well as vigorous latent heating.

b. Forecast from barotropic initialization

The first integration with the P. E. model is a 6-hr forecast from 1800 GMT 4 November to 0000 GMT 5 November using the barotropic initialization. By 0000, the P. E. model shows that most of Lake Erie and the area to the south is covered by ascending motion as seen in Figs. 4–7. The most intense upward motion is taking place at 875 mb over the lakes and at 700 mb over southwestern Pennsylvania and eastern Ohio. At 875 mb the patterns of vertical motion appear to take on a wave-like structure with a wavelength of from 4 to 6 grid intervals. While the Lake Erie Basin is covered with ascending air, only the west-central and northwestern portion of Lake Ontario is covered with ascent, and the depth of the ascending air is limited to 875 and 950 mb. The magnitude of omega at 875 mb over Ontario is only one-half that forecast over portions of Lake Erie. The difference in omega patterns over both lakes probably reflects the residence time of the synoptic trough over the warm waters and the linking of the macroscale and mesoscale baroclinic zones.

Fig. 8 provides a comparison of forecast ascent with observed radar echoes as detected by 10-cm radar at 2345 GMT 4 November. Shading by diagonal lines represents the extent of radar echoes reported by the Detroit, Buffalo and Pittsburgh WSR-57 radars 15 min prior to the barotropic forecast initialization. Significant snow shower activity was limited to an area northwest of extreme western Lake Erie, plus a small patch of echoes over northeastern Ohio at 1745 GMT 4 November. Six hours later, the stippled area shows the rapid spread of convection across most of Lake Erie and its leeward shore, with a broad band of echoes centered on the Ohio-Pennsylvania border. Maximum cloud tops to 10,000 and 13,000 ft appear only in those regions where forecast ascent extends through the 700-mb surface (Fig. 7). The 9000-ft cloud tops over Pittsburgh are within the mesoscale wavelength feature associated with the forecast convergence field as it propagates southeastward from Lake Erie. Cloud tops in the immediate vicinity of Buffalo were limited to 7000 ft.

The forecast patterns of 6-hr snowfall shown in Fig. 9 seem most highly correlated with the ascending omegas and low-level moist inflow. Two small areas of 5-inch snowfall predicted over eastern Lake Ontario occur early in the forecast period. Lingering ascent predicted at the quasi-geostrophic scale by the barotropic model (Fig. 3b) advects beyond Lake Ontario as the associated

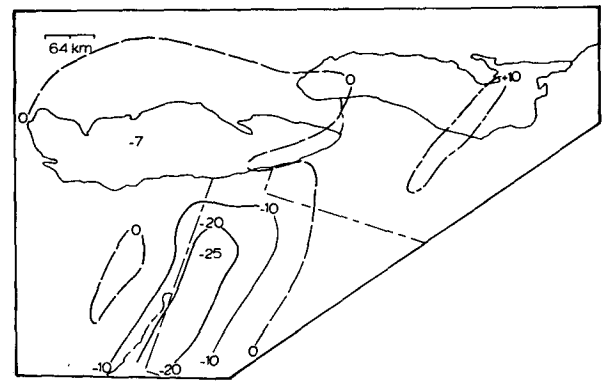

FIG. 6. Same as Fig. 4 except for 800 mb.

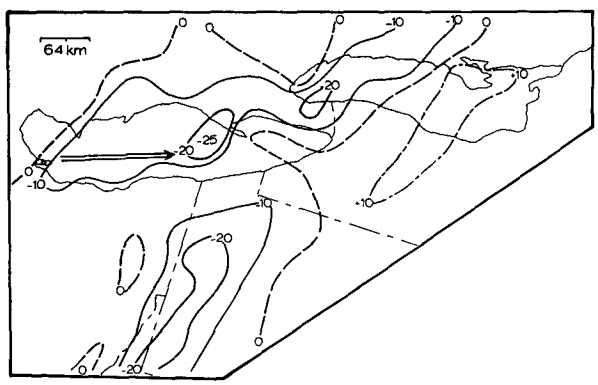

FIG. 5. Same as Fig. 4 except for 875 mb.

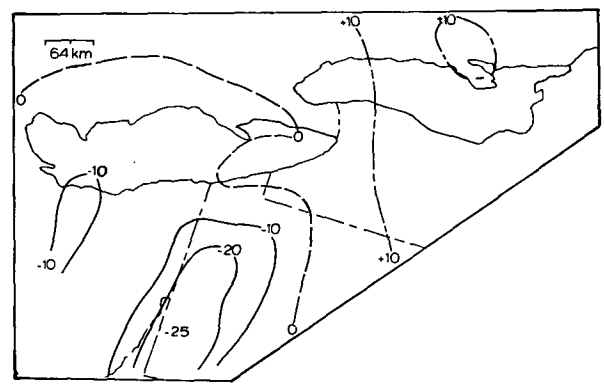

FIG. 7. Same as Fig. 4. except for 700 mb.

Unauthenticated | Downloaded 06/15/24 06:48 AM UTC

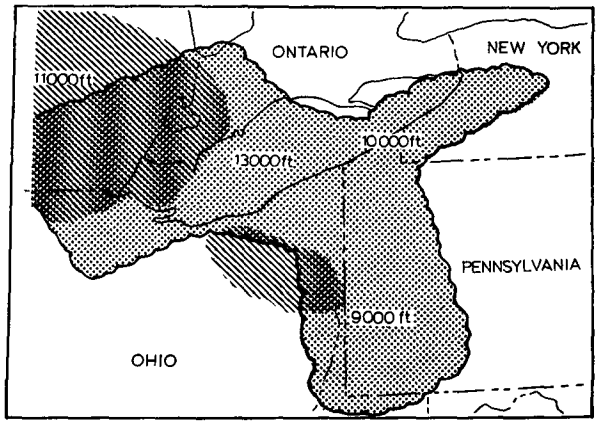

FIG. 8. WSR-57 (10 cm) radar observations from Buffalo, Pittsburgh and Detroit. Diagonal lines represent echoes at 1745 GMT 4 November, 15 min prior to the barotropic initialization. Stippled portion represents echoes 6 hr later.

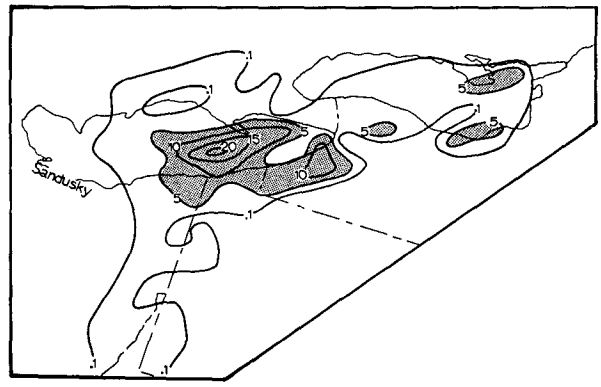

FIG. 9. 6-hr forecast of total snowfall (inches) at 120 time steps from the barotropic initialization at 1800 GMT 4 November.

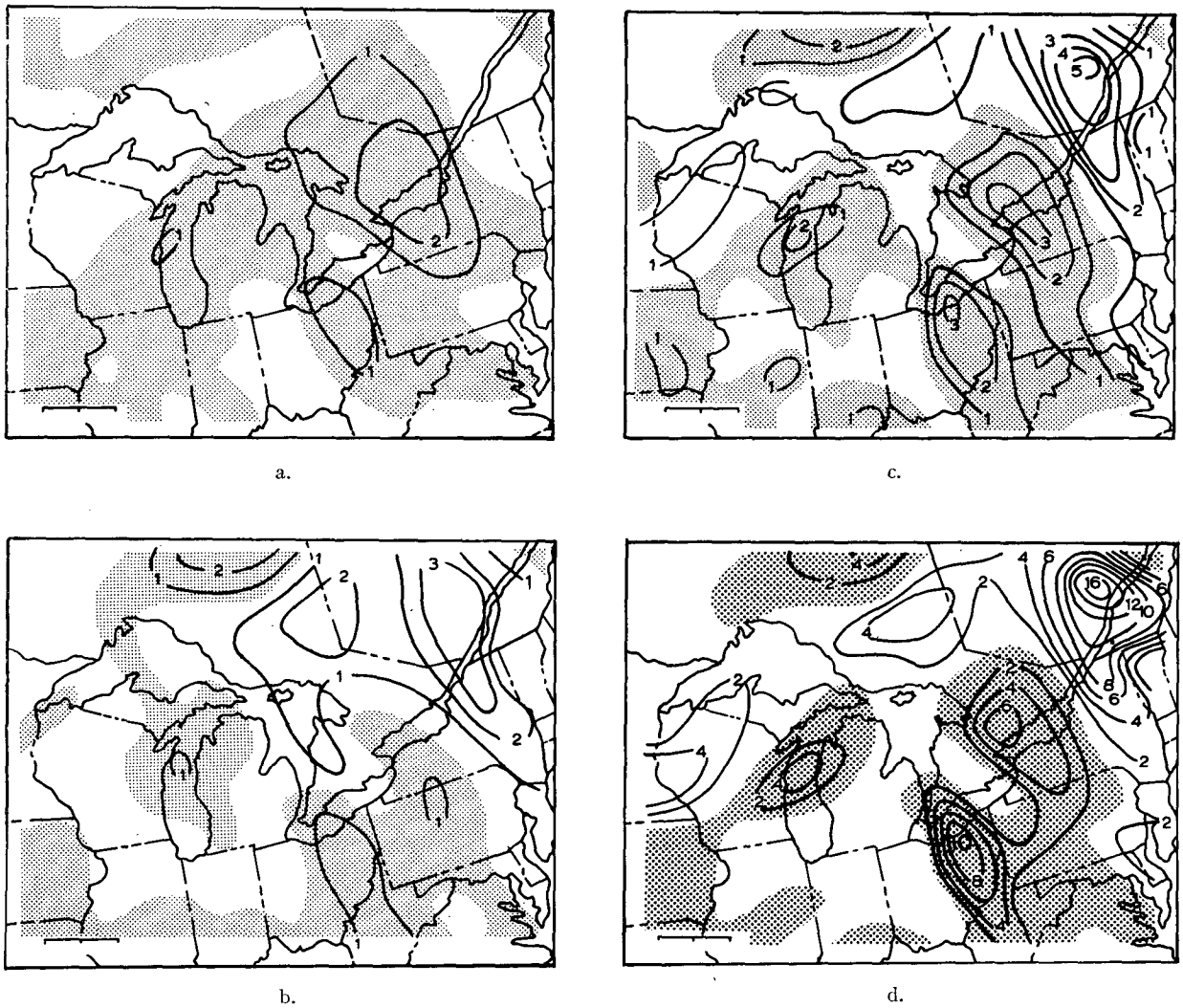

FIG. 10. 800-mb omega (μb sec^{-1}) forced by the vertical variation of vorticity advection, a., by the Laplacian of thickness advection, b., and by their sum, c., at 0000 GMT 5 November 1967. The enhanced omega is given in 10d at the same time.

Unauthenticated | Downloaded 06/15/24 06:48 AM UTC

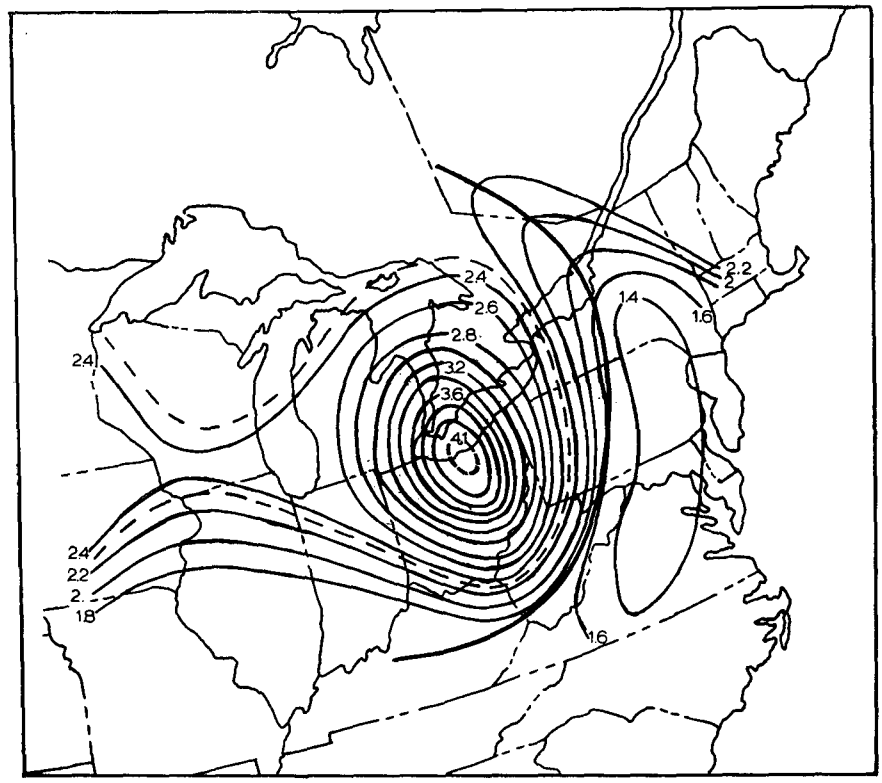

FIG. 11. 800-mb enhancement factor diagnosed at 0000 GMT 5 November.

strong cold front moves into western New England by 0000 GMT 5 November.

The heaviest predicted snowfall, approximately 20 inches in 6 hr, is found near the east-central portion of Lake Erie. This is the area of longest duration of intense upward vertical motion and low-level moist inflow initiated by the secondary trough. It is significant to note that while omegas are stronger over the inland areas south of Lake Erie, the lack of an abundant low-level influx of moisture as well as the rapid movement of this omega field may be responsible for the forecast and observed minimal snowfall amounts (Fig. 2) in this area.

It should also be pointed out that two of the most critical microphysical assumptions concern the snowfall-meltwater ratios and the mean cloud depth. The depth of upward omega determined the cloud depths, (3 km over Lake Erie and 1.67 km over Lake Ontario), while the ratios were assigned to be 15:1 from climatological mapping performed by Jiusto and Kaplan (1972). A cumulus parameterization scheme used within the model is outlined in Appendix B.

c. A comparison with diagnosed quasi-geostrophic omegas

The diagnostic integrations carried out by the quasi-geostrophic model at 0000 GMT 5 November provide a means of comparing *forecast* mesoscale fields with *observed* influences of diabatic heating at the synoptic scale. The 800-mb surface over the Great Lakes is the level of maximum omega calculated on a 127-km grid, near where the release of latent heat was forecast to be most vigorous. These diagnosed patterns of 127-km omega are illustrated in Figs. 10a–d. Shaded areas represent upward motion in microbars per second ($\approx$cm sec^{-1}).

We first note over Lakes Erie and Ontario the similarities in the fields of 800-mb omega when partitioned into vertical motion forced by the vertical variation of vorticity advection (Fig. 10a) and the Laplacian of thickness advection (Fig. 10b). The reinforcement between hydrodynamic forcing and that of substantial thickness increase brought about by the release of latent heat from cumulus towers over the eastern lakes is more prominent when both fields are added together, as shown in Fig. 10c. Finally, Fig. 10d includes the enhancement factor as a means of effectively measuring the transformation of the static stability field at 127 km.

The enhancement factor is the inverse ratio of the observed atmosphere's degree of gravitational damping versus that imposed by the three-dimensional variations of stability found within the standard atmosphere. Thus, the destabilizing effects of the forecast mesoscale wave carrying ascent > -20 μb sec^{-1} from Lake Erie southeastward into Pennsylvania may account for the increase and subsequent elongation of the diagnosed 800-mb enhancement factor across Ohio (Fig. 11).

Likewise, this same index of diabatic heating has

Unauthenticated | Downloaded 06/15/24 06:48 AM UTC

shown a four-fold increase in parcel static energy at the point where -10 μb sec^{-1} ascent is diagnosed upon the 127-km grid over extreme southwestern Lake Erie (Fig. 10d). At 2145 GMT 4 November, the Detroit 10-cm radar record lists isolated thunder-snowshowers breaking out 80 n mi due east over Lake Erie with maximum cloud tops to 15,000 ft observed within the 4.0 isopleth of the enhancement factor shown in Fig. 11. The location of these cells is in line with the maximum predicted mesoscale ascent and snowfall advecting east-northeastward from Sandusky, Ohio, as shown in Figs. 5 and 9.

d. Forecast from the ten-level initialization by the omega equation

The diagnostic data from the 0000 GMT 5 November integration is used as initial data for an 8-hr P. E. forecast. The improved nature of these data (relative to the fields derived by extrapolation from the single-level barotropic forecast) in its depiction of the vertical variation of the geopotential surfaces describes an initial environment more conducive to latent heating and low-

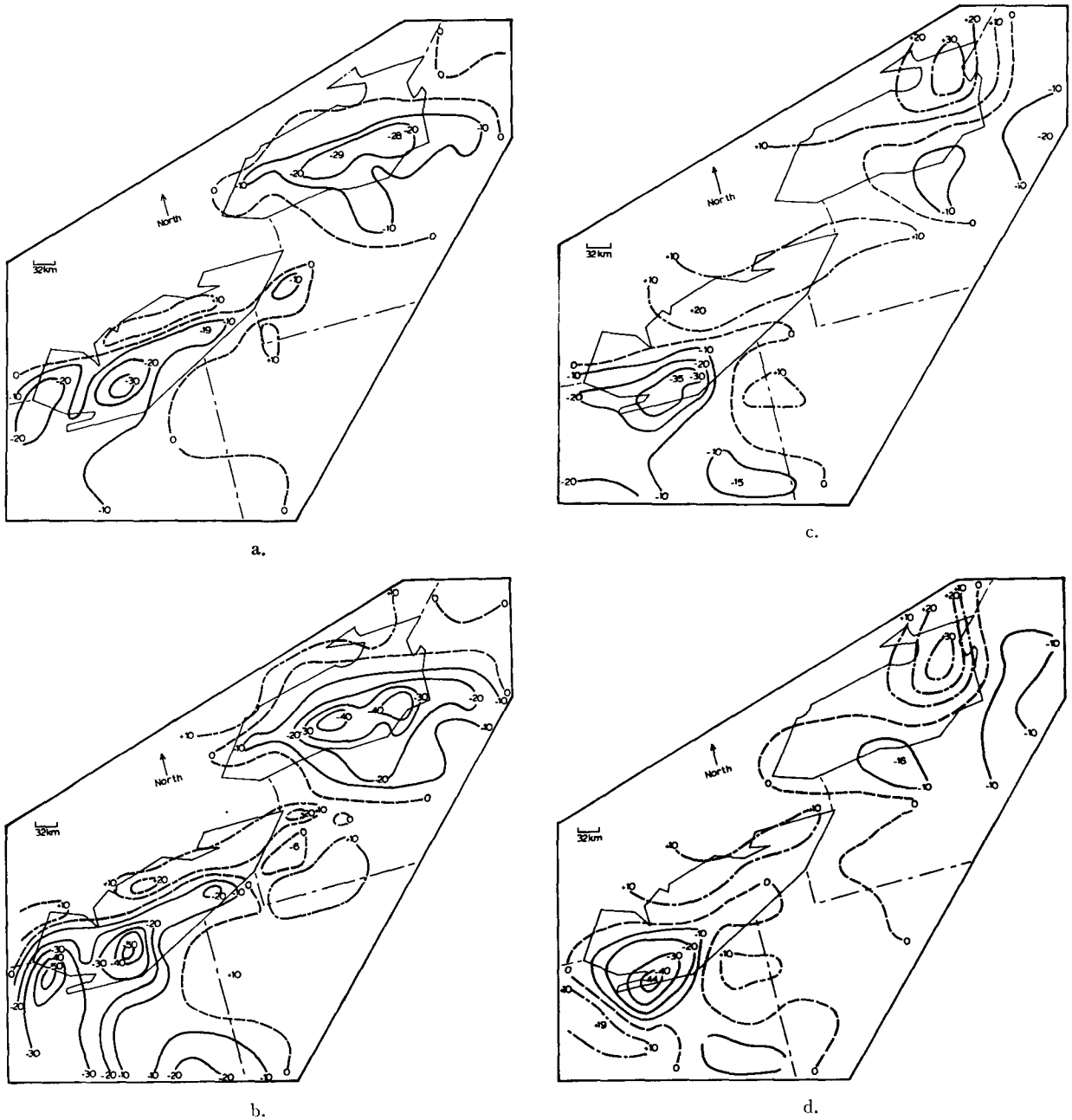

FIG. 12. 150th time-step forecast of 950-, 875-, 800-, and 700-mb omega (μb sec^{-1}), a.–d., respectively, at 0742 GMT 5 November 1967. The P.E. forecast is initialized by the 10-level quasi-geostrophic model.

Unauthenticated | Downloaded 06/15/24 06:48 AM UTC

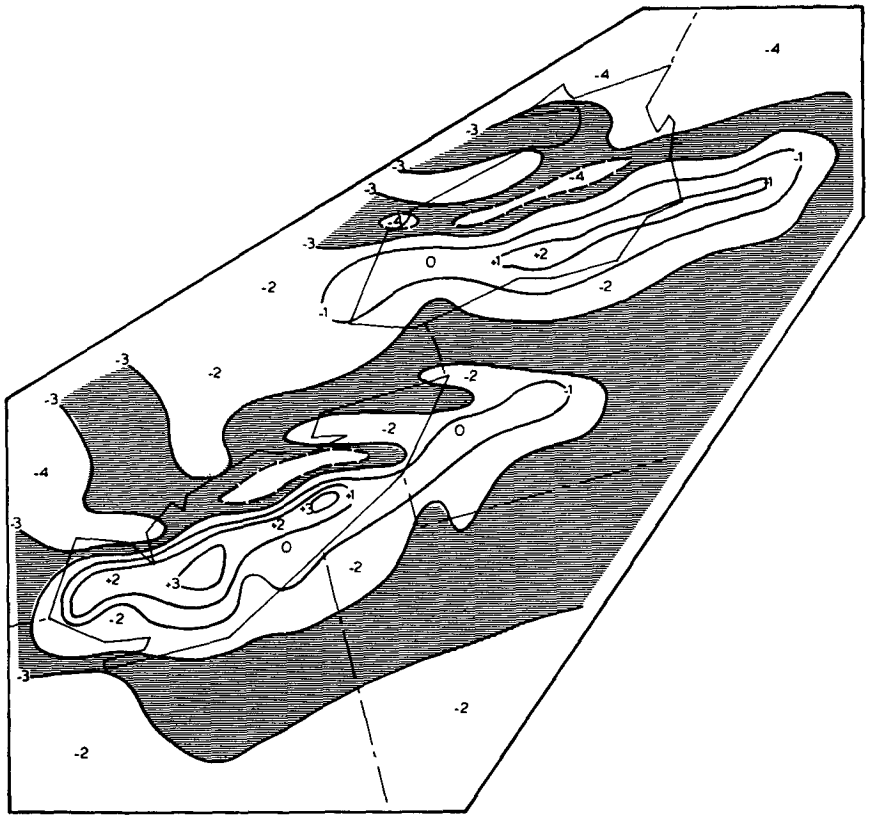

FIG. 13. Forecast 950-mb temperature (°C) field at time step 100.

level heat and moisture flux.[3] By time step 150, vigorous mesoscale vertical motions have developed, notably over Lake Erie (Figs. 12a–d). The omegas, as in the previous integration, were a maximum at 875 mb. Magnitudes in excess of -50 μb sec^{-1}, as seen in Fig. 12b, are forecast over south-central and southwestern Lake Erie.

These omegas should be compared to those derived by Lavoie *et al.* (1970) in which maximum steady-state values of vertical motion approximated 15 cm sec^{-1} coming after nearly 9 hr of integration time. It should be noted, however, that Lavoie's results were for a different lake-effect case study. Lavoie utilized a grid spacing of 6×12 km in the horizontal, with three levels in the vertical.

The contribution to the sloping geopotential surface is considerable from the low-level, lake-induced heat flux. The 950-mb heat anomaly predicted after 100 time steps (Fig. 13) amounts to more than 4C in several areas. The shading of the -3C isothermal field accentuates the warming over both lakes advecting across their leeward shores. This baroclinity, when superimposed upon the pre-existing baroclinity between 800 and 900 mb due to the low-level trough, is sufficient to cause upward vertical motion and significant latent heating.

[3] The quasi-geostrophic initialization will eventually be replaced by a complete nonlinear balance initialization similar to that used by Krishnamurti and Baumhefner (1966).

The resemblance between the patterns of forecast omega with the observed radar pictures, snowfall patterns, and the 1200 GMT 5 November quasi-geostrophic omegas may be seen over Lake Erie. The 0745 GMT 5 November radar observations (Fig. 14) depict 11,000-ft cloud tops over west-central Lake Erie where predicted omegas of -30 to -50 μb sec^{-1} are shown at the four forecast levels seen in Figs. 12a–d. Maximum convective cell tops to 14,000 ft at 1145 GMT 5 November and 16,000 ft at 2345 were reported within this same area. A second area of weaker convection observed south

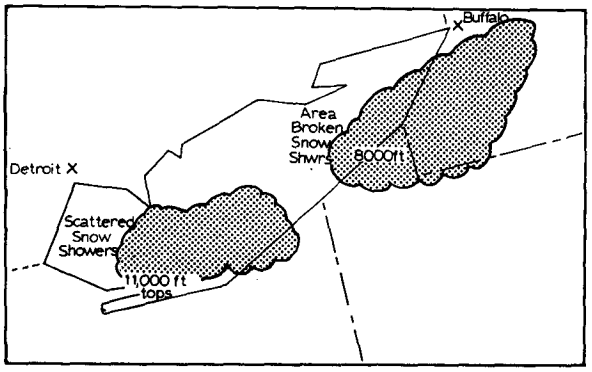

FIG. 14. WSR-57 (10 cm) radar observations at 0745 GMT 5 November corresponding to the P.E. forecast at 150 time steps.

Unauthenticated | Downloaded 06/15/24 06:48 AM UTC

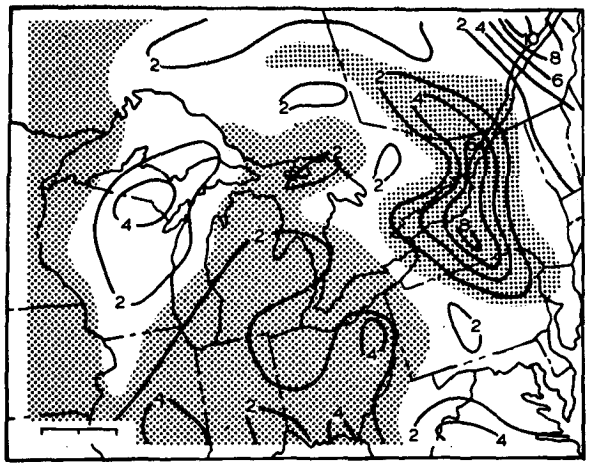

FIG. 15. 800-mb diagnosed enhanced omega (μb sec^{-1}) at 1200 GMT 5 November 1967.

of Buffalo at 0745 is partially defined by the predicted omega fields seen in Figs. 12a and 12b showing 950- and 875-mb ascents corresponding to these cloud patterns.

Four hours later, the diagnosed 1200 GMT quasi-geostrophic omega field at 800 mb (Fig. 15) depicts ascent across Ohio in a manner similar to the predicted P. E. fields, with a second area of vigorous ascent over the eastern half of Lake Ontario. The Buffalo radar is unable to detect lake-effect echoes over eastern Lake Ontario. However, the observed snowfall patterns seen in Fig. 2 show an elongated pattern of heavy accumulation east-southeast of Lake Ontario. The P. E. omega fields in the lower troposphere are basically of similar orientation to this pattern with a general diminishing of intensities and depth over Ontario as opposed to Erie, possibly reflecting the shorter period of convective latent heating.

7. Summary and conclusions

A numerical model has been developed to link quasi-geostrophic and mesoscale forcing functions. This model has shown an ability to simulate the evolution in space and time of the appropriate geophysical fields in an intense lake-effect development. The model is capable of producing vertical motions of greater than 50 cm sec^{-1} within 8 hr and still maintain numerical stability. The initial quasi-geostrophic feature maintains its identity in time while the release of energy stored at smaller scales rearranges the geopotential field. The forecast bulk radiation of energy in the form of long gravitational waves has been supported by upper air observations discussed by Paine and Kaplan (1971).

Acknowledgments. This study was completed through the support of the Atmospheric Sciences Section, National Science Foundation, under Grant GA-35250. Portions of the research were supported by the Atmospheric Physics and Chemistry Laboratory, NOAA, under Grant E22-49-70. The authors gratefully acknowledge the Department of Atmospheric Sciences, State University of New York at Albany, for generous donation of computer time. Thanks also go to Robert Duncan, Frank Brown, Bruce Bendini, Joseph Snyder, and additional employees of the SUNYA computer center facility who gave invaluable assistance to the authors. Ms. Lee and Ms. Grey typed the manuscript.

APPENDIX A

List of Symbols

A, B	horizontal scale factor
C	vertical scale factor
C_1, C_2	low-level moisture flux, condensation functions
C_d	drag coefficient
C_p	specific heat of air at constant pressure
C_{pm}	specific heat of moist air at constant pressure
d	horizontal grid distance
f	Coriolis parameter
f_0	constant value of f
$f(x)$	function of variable x
F_x, F_y	frictional stresses
g	gravitational acceleration
H	scale height
h	vertical increment
H_1, H_2	low-level turbulent flux of sensible heating and latent heating, respectively
I	ideal or standard value of variable
J	Jacobian operator
K_Q, K_H, K_M	exchange coefficients for moisture, heat and momentum
1nd	level of non-divergence
L	latent heating
m	map scale factor
n, m	upper and lower bounds
p, P	pressure
p_1, p_2	pressure levels
P_{300}, P_{950}	pressure surfaces
P_s	surface pressure
Q	mixing ratio
Q_{sat}	saturation mixing ratio
R	gas constant for dry air
R	real value of a variable
T	temperature
T_v	virtual temperature
$\bar{T}_v$	mean virtual temperature
u, v	horizontal wind components
$\mathbf{V}$	total velocity vector
$\mathbf{V}_s$	surface velocity vector
$\mathbf{V}\cdot\nabla$	advection
w	vertical velocity in z system
Z	height of pressure surface
Z_0	surface height
Z_{level}	specific height surface
∇	del, gradient operator

Unauthenticated | Downloaded 06/15/24 06:48 AM UTC

∇^2	Laplacian operator
$\nabla \cdot \mathbf{V}$	divergence
Δ	delta, finite increment in space or time
ΔT, ΔX	increments in T and X
Δc	condensation rate
ϵ	dependent variable
$\partial/\partial x$, $\partial/\partial y$	horizontal space derivative
$\partial/\partial t$	local derivative with respect to time
$\partial/\partial P$	local derivative with respect to pressure
$\partial/\partial z$	local derivative with respect to height
ζ	relative vorticity
Φ	geopotential
ρ	density
ω	vertical velocity (dp/dt) in pressure system
σ	static stability
θ_e	equivalent potential temperature
τ_x, τ_y	horizontal stresses

APPENDIX B

Cumulus Parameterization Scheme

If X is any grid point, then the requirements for adding nonhydrostatic latent heating are:

1) X_{IJK}, X_{I+1JK}, X_{I-1JK}, X_{IJ+1K}, X_{IJ-1K}, X_{IJK+1}, and X_{IJK-1} are all saturated.
2) Above these seven grid points we have a mean ω equal to -20 μb sec^{-1}.
3) The temperature decreases from X_{IJK-1} to X_{IJK+1}.

We assume 30% of the grid box contains convection, where 10% of the grid box has omegas $\sim$10 times the 32-km omega, and 20% has omegas $\sim$5 times the 32-km omega. Upon defining

$$H_{\text{total } L} \approx 2\frac{\omega_{\text{total}}}{\omega_{\text{threshold}}} H_{32\text{km } L} + H_{32\text{km } L},$$

then

$$\omega_{\text{total}} = \omega_{I+1JK} + \omega_{I-1JK} + \omega_{IJ+1K} + \omega_{IJ-1K} + \omega_{IJK+1} + \omega_{IJK-1} + \omega_{IJK},$$

where

$$\omega_{\text{threshold}} = -140 \ \mu\text{b sec}^{-1} \text{ or } (7 \times -20 \ \mu\text{b sec}^{-1}),$$

and

$$H_{32\text{km}L} = \text{latent heating at 32 km.}$$

REFERENCES

Bushby, F. H., and M. S. Timpson, 1967: A ten-level atmospheric model and frontal rain. *Quart. J. Roy. Meteor. Soc.*, **93**, 1–17.

Gerald, C. F., 1970: *Applied Numerical Analysis*. Reading, Mass., Addison-Wesley, 272 pp.

Gerrity, J. P., and R. D. McPherson, 1970: Noise analysis of a limited-area fine mesh prediction model. ESSA Tech. Memo. WBTM NMC-46, 81 pp.

Jiusto, J. E., and M. L. Kaplan, 1972: Snowfall from lake-effect storms. *Mon. Wea. Rev.*, **100**, 62–66.

Kreitzberg, C. W., and H. A. Brown, 1970: Mesoscale weather systems within an occlusion. *J. Appl. Meteor.*, **9**, 417–432.

Krishnamurti, T. N., and D. P. Baumhefner, 1966: Structure of a tropical disturbance based on solutions of a multi-level baroclinic model. *J. Appl. Meteor.*, **5**, 396–406.

Lavoie, R. L., 1968: A mesoscale numerical model and lake-effect snowstorms. Ph.D. thesis, Pennsylvania State University, 102 pp.

——, L. G. Davis, C. L. Hosler and J. I. Kelley, 1970: Investigation of lake-effect storms. Pennsylvania State University Final Rept., ESSA Contract E22-103-68(N), 52 pp.

Matsuno, T., 1966: Numerical integrations of the primitive equations by a simulated backward difference method. *J. Meteor. Soc. Japan*, **44**, 76–83.

McPherson, R. D., 1971: Recent research into numerical methods at the National Meteorological Center. NOAA Tech. Memo. NWS NMC-50, 35 pp.

Nakaya, U., 1954: *Snow Crystals, Natural and Artificial*. Harvard University Press, 510 pp.

Nitta, T., 1962: The outflow boundary condition in numerical time integration of advective equations. *J. Meteor. Soc. Japan*, **40**, 13–24.

Paine, D. A., 1971: The diagnosis and prediction of synoptic-scale influences leading to mesoscale lake-effect development. Ph.D. thesis, State University of New York at Albany, 95 pp.

——, and M. L. Kaplan, 1971: The linking of multiscaled energy sources creating a severe local winter storm. *Preprints, Seventh Conf. Severe Local Storms*, Amer. Meteor. Soc., 299–306.

Petterssen, S., 1956: *Weather Analysis and Forecasting*, Vol. 1. New York, McGraw-Hill, 428 pp.

Sanders, F., and D. A. Olson, 1967: The release of latent heat of condensation in a simple precipitation forecast model. *J. Appl. Meteor.*, **6**, 229–236.

Shuman, F. G., 1957: Numerical methods in weather prediction II. Smoothing and filtering. *Mon. Wea. Rev.*, **85**, 357–363.

Simpson, J., 1968: On some aspects of sea-air interaction in middle latitudes. *Deep Sea Res.*, **16**, 233–261.

Stuart, D. W., and T. H. R. O'Neill, 1967: The overrelaxation factor in the numerical solution of the omega equation. *Mon. Wea. Rev.*, **95**, 303–307.

Thompson, R. D., 1961: *Numerical Weather Analysis and Prediction*. New York, Macmillan, 170 pp.

Unauthenticated | Downloaded 06/15/24 06:48 AM UTC